RSC Advances

PAPER

View Article Online
View Journal | View Issue

Cite this: *RSC Adv.*, 2026, **16**, 26312

Emergency decontamination of leaked unsymmetrical dimethylhydrazine with carboxyl-rich graphene oxide: performance and mechanism

Zuozhou Hou, Yuanzheng Huang,* Ying Jia, Lurong Du, Diwen Zheng, Wenwen Li, Xuan Ling, Keke Shen and Guofeng Jin

Unsymmetrical dimethylhydrazine (UDMH) is a widely used high-energy liquid propellant known for its extreme flammability and explosiveness. During storage or handling, any leakage of UDMH poses significant safety risks due to its volatility and reactivity, potentially resulting in fire or detonation. Conventional water spray methods are inefficient and consume excessive water, underscoring the urgent need for advanced decontamination techniques to address UDMH leaks. Graphene oxide (GO) presents a promising solution due to its unique two-dimensional nanoscale structure and adjustable surface functional groups, which enhance molecular capture capabilities. In this study, an aqueous dispersion of GO at a concentration of 18 mg mL^{-1} was synthesized using a modified Hummers' method and further functionalized through carboxylation *via* an S_N2 nucleophilic substitution mechanism. The morphological and structural properties of the resulting material were systematically characterized using SEM, TEM, XRD, Raman, FT-IR, and XPS. The carboxyl-rich graphene oxide demonstrated strong inhibitory effects on UDMH vapor release, primarily through chemical adsorption. Specifically, 4 mL of the modified GO achieved a 23.1% inhibition efficiency against UDMH emissions from a 0.5 g L^{-1} solution. To improve decontamination performance, the decontaminant was formulated with Lewis acidic metal ions and the surfactant sodium dodecylbenzenesulfonate (SDBS). Metal ions such as Fe^{3+} and Cu^{2+} improved inhibition through acid–base neutralization, *in situ* coordination reactions, and interfacial modulation. Results showed that 10 mmol L^{-1} Fe^{3+} increased the inhibition rate to 36%, while 90 mmol L^{-1} Cu^{2+} raised it to 32.4%. SDBS contributed through micelle formation and interactions with the organic components of UDMH, enabling 0.5 g L^{-1} of SDBS to boost inhibition to 35.1%. This work demonstrates the potential of functionalized graphene oxide-based formulations as effective decontamination agents for hazardous energetic substances, offering a viable strategy for emergency response to energy leaks.

Received 5th February 2026
Accepted 11th April 2026

DOI: 10.1039/d6ra01033d

rsc.li/rsc-advances

Introduction

The advancement of science and technology, along with increased exploration in space launches, has led to a rising demand for high-energy liquid propellants, such as unsymmetrical dimethylhydrazine (UDMH).[1,2] Although UDMH is known for its flammability, explosiveness, and high toxicity, it has a boiling point of only 63.9 °C and a flash point as low as −15 °C. The International Agency for Research on Cancer (IARC) of the World Health Organization has classified UDMH as a Group 2B carcinogen.[3] When released into the environment or stored under uncontrolled conditions, UDMH readily forms a range of toxic transformation products, such as monomethylamine, dimethylamine, and *N*-nitrosodimethylamine.[4] These byproducts may even lead to explosions, posing a significant threat to ecological and public safety. Such incidents highlight the randomness, complexity, and high hazard associated with UDMH leakage, suggesting that current emergency response methods are inadequate to mitigate potential harm. Therefore, the development of more effective emergency response strategies is critically important.

Currently, researchers worldwide are highly interested in UDMH wastewater treatment. Advances in UDMH degradation technologies are ongoing. For instance, Li *et al.* synthesized the catalyst CO-ZF-4%/BC to activate PDS through high-pressure hydrothermal pyrolysis, achieving a degradation efficiency of 90.4% for UDMH.[5] Su *et al.* synthesized FCZ@C-600 with a maximum adsorption capacity of 185.70 mg g^{-1} for UDMH using layer-by-layer self-assembly and pyrolysis.[6] Zeng *et al.* developed a 001-TiO_2/CeO_2 S heterojunction primarily composed of the (001) plane *via* a solvothermal-photoassisted method. This system achieved a 98.7% degradation efficiency for 100 mg L^{-1} UDMH wastewater under simulated sunlight

Rocket Force University of Engineering, Xi'an 710025, China. E-mail: huangyzxa@163.com

within 140 minutes.[7] Nevertheless, studies on emergency response measures for UDMH leaks are scarce.[8,9] Common strategies for emergency mitigation of UDMH leakage include source plugging,[9,10] adsorption,[11,12] and water spray methods.[13,14] The water spray approach employs water curtains to absorb UDMH and slow its diffusion.[15] Because it is easy to deploy and yields a rapid response, this method is widely used in practice. However, this method not only requires a large volume of water but also allows absorbed UDMH to re-volatilize, creating an explosion hazard. Therefore, improving this technology to suppress UDMH volatilization and to provide more favorable conditions and sufficient time for subsequent emergency response is of great significance.

Graphene oxide (GO) offers distinct advantages and broad application potential among advanced materials due to its two-dimensional layered structure, abundant surface oxygen-containing functional groups, excellent solution dispersibility, facile functionalization, and potential for low-cost, large-scale synthesis.[16–18] It has been widely investigated for pollutant control. In this study, taking advantage of GO's amenability to functional modification, we performed carboxylation to introduce a high density of carboxyl groups onto its surface, a change that markedly improves hydrophilicity, dispersibility, and chemical reactivity.[8,19,20] Targeting the escape and diffusion behavior of UDMH, we systematically designed and optimized a series of GO-based decontaminant substrates aimed at inhibiting UDMH release. A low-cost, economically viable, safe, and highly efficient liquid adsorption material for spray-based treatment was developed, markedly improving the performance of water spray methods in emergency disposal UDMH leakage. This study effectively reduced the risk of explosion caused by UDMH leakage, providing more favorable conditions and sufficient time for further disposal. This work serves as a valuable reference for emergency responses to incidents involving special fuel leakage.

Experimental section

Materials

Hydrochloric acid (37 wt%), chloroacetic acid, copper nitrate trihydrate (AR)and ferric nitrate nonahydrate (AR) were produced from Adamas; sulfuric acid (98 wt%), potassium permanganate (AR) and sodium dodecylbenzene sulfonate (AR) were purchased from Greagent; sodium nitrite (AR) were obtained from Tianjin Comate; 3% hydrogen peroxide solution (AR) were purchased from Qingdao Rishui; nano graphite powder (AR)were obtained from Xianfeng Nano Technology Co., Ltd; UDMH of 98 wt% purity was obtained from Qinghai Liming Chemical Co., Ltd (Xining, China); all water used was ultrapure water (≥18.25 MΩ cm) prepared by UPWS-I-10T ultrapure water system produced by Chongqing Senyuan Purification Technology Co., Ltd; all substances were used directly without further purification.

Synthesis of carboxyl-rich graphene oxide

GO solution was synthesized *via* the modified Hummers' method, followed by functionalization through an S_N2 reaction mechanism to introduce a high density of carboxyl groups preferentially at the edge sites of GO. The detailed synthesis procedure is as follows: 0.5 g of GO powder was dispersed in 500 mL of deionized water in a 1000 mL beaker and subjected to ultrasonic treatment for 1 h to achieve a homogeneous dispersion. Subsequently, 7.5 g of chloroacetic acid was added, and the mixture was reacted under simultaneous ultrasonication and stirring for 3 h to promote efficient nucleophilic substitution. Upon completion of the reaction, the product was thoroughly purified by repeated centrifugation with deionized water to remove unreacted reagents and by-products. Finally, the purified material was collected and freeze-dried to yield carboxyl-rich graphene oxide with enhanced surface functionality.

Characterizations of GO and carboxyl-rich GO

The morphology of GO and carboxyl-rich GO was characterized using scanning electron microscopy (SEM, GeminiSEM 360) and transmission electron microscopy (TEM, JEM-2100 F UHR). Structural features were analyzed by X-ray diffraction (XRD, D8 Advance) and Raman spectroscopy (InVia Reflex). Fourier transform infrared spectroscopy (FT-IR, IRTracer 100) and X-ray photoelectron spectroscopy (XPS, ESCALAB Xi+) were employed to investigate the functional group composition and chemical states of the materials, respectively.

Decontamination performance evaluation

An experimental platform was constructed in this study, consisting of a 500 mL single-neck round-bottom flask as the reaction vessel, a constant-temperature water bath for temperature control, and a UDMH gas detector as the analytical device. Experiments were conducted at a controlled temperature of 25 °C, with the apparatus schematic presented in Fig. 1. A 0.5 g L^{-1} UDMH solution was uniformly employed across all trials to investigate the effects of various factors on decontamination performance.

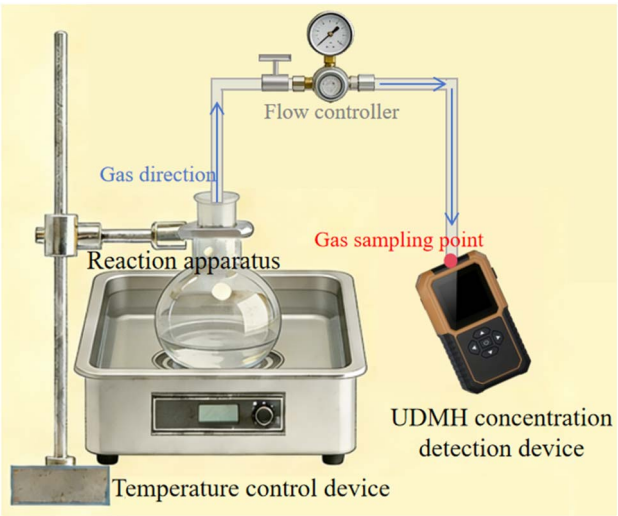

Fig. 1 Apparatus schematic.

The experimental procedure was as follows: first, 100 mL of the UDMH solution was added to the flask, followed by thorough stirring and stewing until gas–liquid equilibrium was achieved. The concentration of UDMH in the gas phase was then measured by portable UDMH gas detector. Subsequently, the decontaminating agent was introduced, and the mixture was again stirred thoroughly and allowed to equilibrate to gas–liquid equilibrium, with a second measurement of the gas-phase UDMH concentration. The efficacy of the material was validated by comparing the gas-phase UDMH concentrations before and after the addition of the contaminant.

The portable UDMH gas detector utilized in this study has a measurement range of 0–1000 ppm and an accuracy of 0.1 ppm, as detailed in the apparatus diagram. To mitigate the environmental impact of UDMH-containing wastewater, oxalic acid was employed for post-experimental solution treatment. For quantitative evaluation of the inhibition efficiency, the escape inhibition rate was calculated using eqn (1).

$$N = \frac{C_0 - C_t}{C_0} \times 100\% \quad (1)$$

Among them, N is the gas escape suppression rate; C_0 represents the initial concentration of UDMH in the bottle. C_t represents the concentration of UDMH after the addition of the detergent.

Theoretical analysis method

To quantitatively evaluate the inhibition efficiency, this study employs the Henry's law constant as a direct indicator of UDMH's tendency to volatilize from the liquid phase to the gas phase—an approach that enables intuitive characterization of escape behavior. The value of Henry's constant can usually be obtained through two main methods: experimental measurement and theoretical estimation. This study mainly adopts the Henry constant H obtained through theoretical calculation based on experimental data. The specific calculation method is as follows:

$$H = \frac{P}{C} \quad (2)$$

$$\frac{P}{P^*} = \frac{C_i}{C^*} \quad (3)$$

$$P = \frac{P^*}{C^*} \times C_i \quad (4)$$

$$k = \frac{H_{0i}}{H_{li}} \quad (5)$$

$$H_{0i} = \frac{p_0}{C_0} = \frac{P^*}{C^*} \times C_{0i} \quad (6)$$

$$H_{li} = \frac{p_l}{C_l} = \frac{P^*}{C^*} \times C_{li} \quad (7)$$

In formula (2), H is the Henry's constant, P is the partial pressure of the gas, and C is the liquid – phase concentration. From the ideal gas partial pressure formula, we obtain formula (3). In formula (3), is the total pressure of the gas phase, and is the total concentration of the gas phase. Therefore, the gas – phase concentration measured by the gas detector can be converted into the gas – phase partial pressure using the partial pressure formula, as shown in formula (4). Given that at 25 °C, is 101 kPa and is 0.5 g L^{-1}, the value of the gas – phase partial pressure can be calculated based on the gas – phase concentration measured by the UDMH gas detector. Theoretically, the value of C in formula (2) is equal to that of in formula (3). However, due to certain errors in the preparation of the unsymmetrical dimethylhydrazine (UDMH) solution, to further reduce the impact of these errors, the theoretical calculation part of this experiment is optimized. The specific optimization formula is presented in eqn (5). The variable k is introduced to quantify the variation of the Henry coefficient. Here, H_{0i} represents the Henry coefficient at the initial equilibrium concentration at 1 h, and H_{li} denotes the Henry coefficient at the equilibrium concentration after decontaminant addition at 2 h. When the value of k is greater than 1, it indicates that the performance of the added decontaminant is effective, decreasing the gas – phase equilibrium concentration before and after, and thus increasing the ratio of the Henry's coefficients before and after. Moreover, the larger the value of k, the better the decontamination performance. The specific steps for data calculation are shown in formulas (6) and (7). Among them, is the initial gas partial pressure; is the gas partial pressure after adding the decontaminant; and are both liquid concentrations; is the concentration of the UDMH gas measured at the initial equilibrium at 1 h; is the concentration of the UDMH gas measured after the equilibrium at 2 h after adding the decontaminant.

Results and discussion

Structure and morphologies of the graphene oxide and carboxyl-rich graphene oxide

The morphologies of graphene oxide (GO) and carboxyl-rich GO were characterized and comparatively analyzed *via* scanning electron microscopy (SEM) and transmission electron microscopy (TEM). As shown in Fig. 2a–d, SEM micrographs reveal that pristine GO exhibits a typical large-area, irregularly wrinkled sheet-like structure with relatively extended but loosely stacked layers. At a magnification corresponding to a 2 nm scale bar, the layer surfaces appear relatively smooth with gently undulating wrinkles. In contrast, the introduction of abundant carboxyl groups induces a fundamental morphological transformation in carboxyl-rich GO: the sheets display a higher degree of distortion, curling, and denser wrinkling, forming a significantly more refined and complex three-dimensional porous network. TEM observations (Fig. 2e–h) show that GO consists of large-sized, continuous sheets with tightly stacked structures, flat surfaces, and mild edge wrinkling. This morphology indicates strong interlayer van der Waals forces, which promote aggregation and may reduce the specific surface area and accessibility of active sites. By comparison, carboxyl-rich GO features distinctly different characteristics: its sheets are

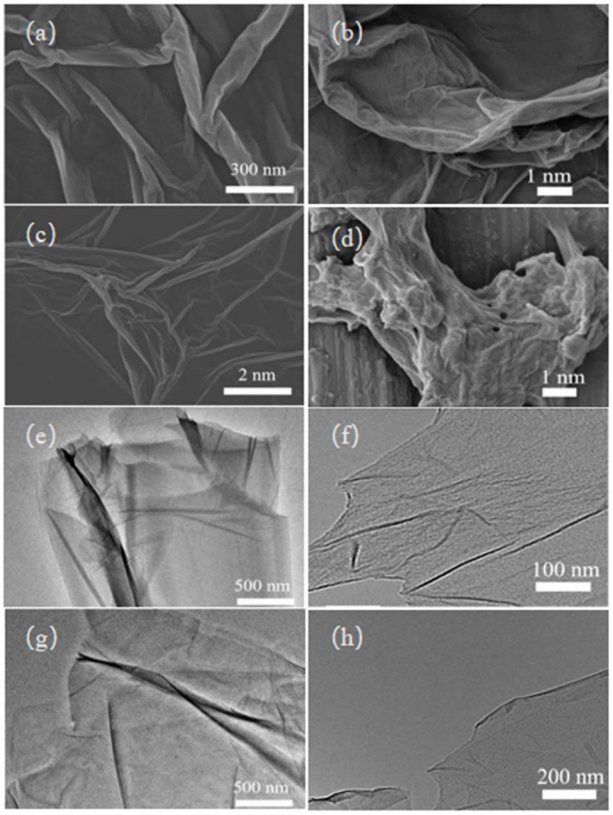

Fig. 2 SEM images of (a) and (c) GO, (b) and (d) carboxyl-rich GO; TEM images of (e) and (g) GO, (f) and (h) carboxyl-rich GO.

fragmented into smaller, more discrete units, and the wrinkling degree is significantly enhanced, resulting in a highly distorted, curled open porous network. Such a structure not only increases the number and accessibility of surface active sites but also substantially improves interfacial mass transfer efficiency, consistent with previous reports.[21,22]

Structural characterization of GO and carboxyl-rich GO was performed using X-ray diffraction (XRD) and Raman spectroscopy. As shown in Fig. 3a, GO exhibits a strong diffraction peak at $2\theta = 12.30°$, corresponding to an interlayer spacing of 7.19 Å. In contrast, carboxyl-rich GO displays a shifted diffraction peak at $2\theta = 10.99°$, with an expanded d-spacing of 8.04 Å. This increase in interlayer distance confirms the successful incorporation of carboxyl groups, which enhances ion and molecular diffusion pathways and thereby improves adsorption capacity in practical applications. Raman spectra (Fig. 3b) reveal that the $I(D)/I(G)$ ratio increases from 0.93 for GO to 0.96 for carboxyl-rich GO. The higher defect density indicated by this ratio suggests a greater concentration of structural defects introduced by carboxyl functionalization, which may serve as additional active sites and promote catalytic activity. The functional groups and chemical compositions of GO and carboxyl-rich GO were systematically analyzed and compared using Fourier-transform infrared spectroscopy (FTIR) and X-ray photoelectron spectroscopy (XPS). As shown in Fig. 3c, FTIR spectra reveal that GO exhibits a broad absorption band at 3408 cm^{-1}

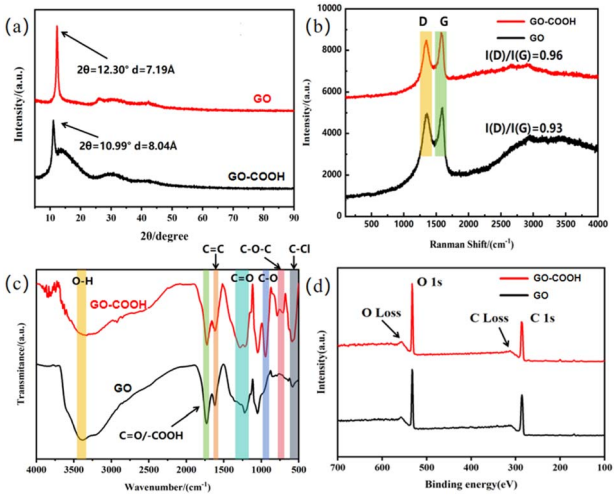

Fig. 3 XRD (a), Raman (b), FT-IR (c) and XPS (d) images of GO and carboxyl-rich GO.

attributed to O–H stretching vibrations, a distinct peak at 1728 cm^{-1} corresponding to C=O and –COOH stretching modes, a signal at 1606 cm^{-1} associated with aromatic C=C skeletal vibrations, and an additional peak at 1215 cm^{-1} due to epoxy C–O stretching. These features confirm the successful incorporation of oxygen-containing functional groups on both the basal planes and edges of GO, which significantly enhances its hydrophilicity and colloidal dispersibility in aqueous media. In contrast, carboxyl-rich GO shows a reduced intensity in the O–H stretching region, accompanied by a pronounced increase in the C=O stretching signal, indicating effective carboxylation *via* covalent grafting of –COOH groups onto the GO framework. Furthermore, a strong and broad absorption band emerges at approximately 952 cm^{-1}, along with enhanced C–O stretching vibrations, suggesting the concurrent introduction of additional functional moieties such as ether (C–O–C) and possibly C–Cl bonds during the carboxylation process. As shown in Fig. 3d, the O 1s core-level peak in carboxyl-rich graphene oxide is significantly intensified relative to pristine GO, indicating a substantial increase in overall oxygen content. Furthermore, the attenuation of the C Loss peak intensity is clearly observed, which is commonly associated with improved electrical conductivity due to reduced graphitic domain disruption or defect saturation. This enhancement in electronic properties may play a crucial role in facilitating electron transfer processes, thereby potentially contributing to superior catalytic performance.[23] To quantitatively assess the surface functional group distribution, high-resolution C 1s spectra of both GO and carboxyl-rich GO were deconvoluted using peak-fitting analysis (Fig. 4). Five distinct components were identified: C=C (sp^2 carbon) at 282.52 eV, C–C (sp^3 carbon) at 283.55 eV, C–O/C–O–C at 284.79 eV, C=O at 285.83 eV, and O–C=O (carboxyl/carbonyl) at 286.51 eV. The presence and relative intensities of these peaks provide direct evidence of diverse oxygen-containing functional groups on both materials, with a notably higher proportion of carboxyl species in the modified sample.

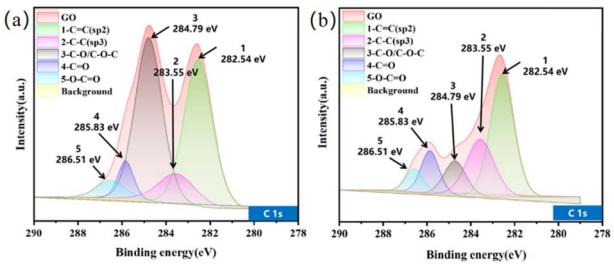

Fig. 4 C 1s X-ray photoelectron spectrum of GO (a) and carboxyl-rich GO (b).

This enriched surface chemistry contributes to enhanced surface wettability and water adsorption capacity, further supporting improved interfacial interactions in aqueous environments.[24]

In addition, the ratio of oxidized carbon species (including C–O–C/C–OH, O–C=O, and C=O) to intact carbon domains (C–C/C=C) in carboxyl-rich graphene oxide, denoted as IOC/ICC, is determined to be 1.86. This value indicates a significantly enhanced oxidation level, which contributes to improved colloidal dispersion stability and increased surface chemical reactivity, likely due to the higher density of polar functional groups that promote interfacial interactions in aqueous media.[25]

Inhibitory effect of carboxyl-rich graphene oxide on decontamination performance

To evaluate the efficacy of carboxyl-rich graphene oxide as a decontaminant in suppressing the volatilization of UDMH, this study employed GO as a comparative material. The results are presented in Fig. 5. Six experimental groups were conducted with incremental additions of GO and carboxyl-rich graphene oxide ranging from 1 mL to 6 mL, and the escape inhibition rate was calculated to assess and compare their effectiveness in mitigating UDMH emission. As shown in the Fig. 5b, all GO-treated groups exhibited negative inhibition rates, indicating minimal suppression of UDMH gas release. In contrast, the carboxyl-rich graphene oxide treated groups consistently yielded positive inhibition rates, peaking at 23.1% when 4 mL of carboxyl-rich graphene oxide was introduced. This observation demonstrates that carboxyl-rich graphene oxide effectively reduces the initial UDMH concentration within the sealed system and significantly inhibits its gaseous escape. The superior performance of carboxyl-rich graphene oxide may be attributed to several synergistic mechanisms. First, unlike GO, which exhibits an inhomogeneous distribution of oxygen-containing functional groups, the abundant surface carboxyl groups on carboxyl-rich graphene oxide can form coordination bonds with the amino groups of UDMH, thereby enhancing both adsorption efficiency and chemical affinity. Second, the functionalization process may generate additional microporous or mesoporous structures on the GO-COOH surface,[26,27] strengthening physical confinement of UDMH molecules. Furthermore, carboxyl-rich graphene oxide can act as a proton donor, promoting the hydrolysis of UDMH and facilitating its oxidative degradation—processes that collectively contribute to the suppression of UDMH volatilization.

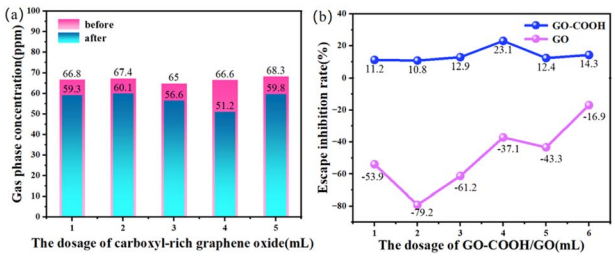

Fig. 5 (a) The influence of the dosage of carboxyl-rich GO on the inhibition of UDMH escape, (b) the escape inhibition rate of GO and carboxyl-rich GO on UDMH.

Effect of metal ion on decontamination performance

The interaction between Lewis acids and carboxyl-rich graphene oxide and UDMH would have a significant impact on the decontamination performance.[28] In this study, $Cu(NO_3)_2 \cdot 3H_2O$ and $Fe(NO_3)_3 \cdot 9H_2O$ were selected as representative Lewis acid metal ion sources and were combined with carboxyl-rich graphene oxide to investigate their effects on UDMH decontamination. A single-factor experimental design was employed to systematically evaluate the impact of varying metal ion concentrations. Under consistent conditions with 4 mL of carboxyl-rich graphene oxide added, 1 mL of either Cu^{2+} or Fe^{3+} solution was introduced at concentrations of 10, 30, 50, 70, and 90 mmol L^{-1}, respectively. The decontamination efficacy was quantified by calculating the UDMH escape inhibition rate.

As shown in Fig. 6, for both Cu^{2+} and Fe^{3+}, the UDMH escape inhibition rate initially decreases within a certain concentration range as the ion concentration increases. This trend is

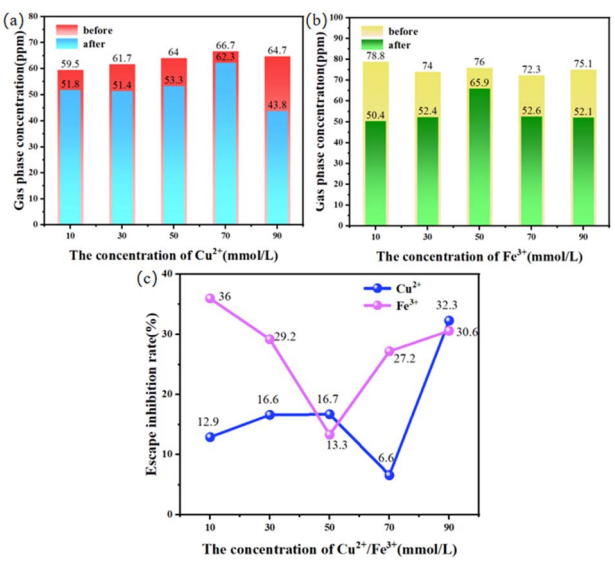

Fig. 6 The influence of the dosage of Cu^{2+} (a) and Fe^{3+} (b) on the escape inhibition of UDMH, (c) comparison of escape inhibition rate.

attributed to coordination site saturation on the graphene oxide surface, hydrolysis of the metal ions leading to surface passivation, and potential competitive side reactions that reduce active site availability.[29–31] However, at this stage, Cu^{2+} promotes the release of UDMH, whereas Fe^{3+} exerts a synergistic inhibitory effect on UDMH release. This difference may be attributed to the fact that, although both metal ions—Cu^{2+} and Fe^{3+}—coordinate with carboxyl groups and thereby disrupt the original adsorption system under low-concentration conditions, Fe^{3+} possesses a higher charge density, resulting in stronger coordination with carboxyl groups. Consequently, the Fe^{3+}-carboxyl coordination complex formed may exhibit a greater affinity for UDMH compared to carboxyl groups alone. Upon further increasing the metal ion concentration, the inhibition rate rises again. This may be because as the concentration increases, Fe^{3+} and Cu^{2+}, acting as Lewis acids, accept the lone–pair electrons on the nitrogen atoms in UDMH molecules to form complexes, thereby inhibiting the escape of UDMH.[32] Additionally, elevated concentrations of Cu^{2+} and Fe^{3+} can promote the *in situ* coordination reaction of metal ions to proceed in the forward direction, thereby enhancing the adsorption capacity for UDMH. High ion concentrations may also induce aggregation of the nanomaterials, altering interfacial properties and further restricting UDMH release.[33,34] The optimal inhibition was observed at 90 mmol L^{-1} for Cu^{2+} and 10 mmol L^{-1} for Fe^{3+}. Overall, the average UDMH escape inhibition rates were 18.28% for Cu^{2+} and 27.7% for Fe^{3+}, indicating that Fe^{3+} exhibits superior performance in enhancing decontamination efficiency. This superiority may be attributed to Fe^{3+}'s stronger oxidative capability, greater propensity to form reactive surface species, and favorable coordination behavior with carboxyl groups.[35,36]

Effect of surfactant on decontamination performance

The specific adsorption behavior of surfactants can significantly influence the performance of decontamination systems.[37] In this study, sodium laurylbenzenesulfonate (SDBS) was selected as a model surfactant to investigate its synergistic effects with carboxyl-rich graphene oxide. SDBS is capable of accumulating at aerosol interfaces and forming reverse micelle structures,[38] which effectively restrict mass transfer of water molecules across the water–air interface. Keeping all other experimental conditions constant, SDBS was introduced into the system at concentrations of 0.2 g L^{-1}, 0.5 g L^{-1}, 1 g L^{-1}, and 3 g L^{-1}. The results, presented in Fig. 7, reveal that the efficacy of UDMH vapor suppression varies with SDBS concentration, reflecting distinct interaction mechanisms between SDBS and carboxyl-rich graphene oxide.

At low concentrations, the delamination and dispersion effect of SDBS on graphene oxide sheets is limited due to insufficient surfactant coverage. Under these conditions, SDBS fails to fully encapsulate the nanosheets or prevent their aggregation. Moreover, it may preferentially bind to carboxyl functional groups on the graphene oxide surface, thereby occupying active sites that would otherwise participate in UDMH capture. This competitive adsorption reduces the availability of binding sites and consequently diminishes the overall inhibition of UDMH volatilization. In an optimal concentration range, however, SDBS boosts the dispersion stability of carboxyl-rich graphene oxide and promotes interfacial spreading, leading to improved suppression of UDMH escape. This synergistic effect is likely attributed to the formation of a composite physical barrier through cooperative assembly at the interface,[39] which hinders both molecular diffusion and evaporation. When the SDBS concentration exceeds this optimal range, the inhibitory efficiency declines. This reduction may result from micelle formation competing with surface adsorption, alterations in interfacial properties that disrupt effective barrier formation, and saturation of available adsorption sites[40,41]—factors that collectively impair system performance.

Study on gas–liquid equilibrium law in reaction system

This study, based on the experimental data, proposes a possible mechanism of action as shown in Fig. 8, and determines the Henry coefficient to derive the *K* value, which provides a more intuitive and accurate representation of the tendency for UDMH to volatilize from the liquid phase into the gas phase. The calculated *K* values are presented in Table 1.

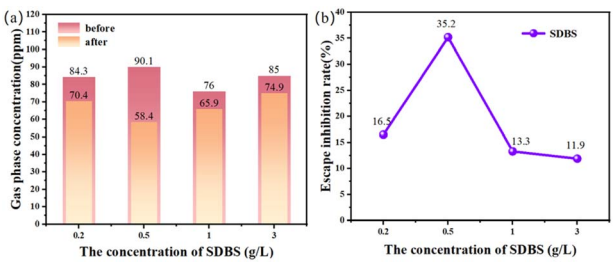

Fig. 7 (a) The influence of the dosage of SDBS on the inhibition of UDMH escape, (b) the escape inhibition rate of SDBS.

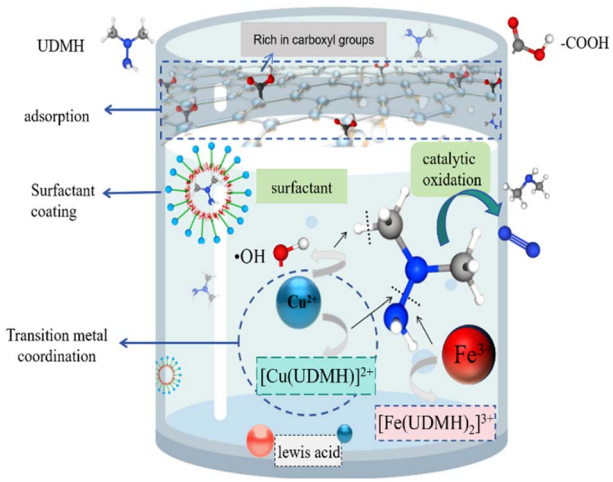

Fig. 8 The escape inhibition mechanism of unsymmetrical dimethylhydrazine.

Table 1 The K value under different conditions

Condition	K
4 ml carboxyl-rich graphene oxide	1.30
4 ml carboxyl-rich graphene oxide +90 mmol L^{-1} Cu^{2+}	1.48
4 ml carboxyl-rich graphene oxide +10 mmol L^{-1} Fe^{3+}	1.56
4 ml carboxyl-rich graphene oxide +0.5 g L^{-1} SDBS	1.54

The calculation results indicate that both the addition of carboxyl-rich graphene oxide and its formulation with Cu^{2+}, Fe^{3+}, and SDBS lead to a decrease in the Henry coefficient of UDMH in solution, accompanied by an increase in the K value. These changes provide theoretical support for the inhibitory effect of carboxyl-rich graphene oxide and its composite systems on the volatilization of UDMH from aqueous media.

Conclusions

This study systematically investigates the gas-phase escape and diffusion behavior of UDMH. Carboxyl-rich graphene oxide was synthesized using a modified Hummers' method combined with S_N2 nucleophilic substitution. Its morphological and structural characteristics were analyzed using SEM, TEM, XRD, Raman spectroscopy, FT-IR, and XPS. The material exhibits a highly distorted, curled, and open porous network architecture, with a higher density of structural defects and increased oxygen-containing functional groups compared to pristine graphene oxide, leading to enhanced oxygen content. Experimental results indicate that UDMH retention is improved through synergistic adsorption and surface functionalization mechanisms, effectively suppressing secondary UDMH emissions. Specifically, 4 mL of carboxyl-rich graphene oxide achieves an inhibition efficiency of 23.1% for UDMH vapor release from a 0.5 g L^{-1} aqueous solution. The decontamination performance is further enhanced by formulating the material with Lewis acid metal ions and surfactants. Metal ions such as Fe^{3+} and Cu^{2+} strengthen adsorption and synergistically inhibit UDMH escape through acid–base neutralization, *in situ* coordination reactions, and interfacial modulation. For instance, 10 mmol L^{-1} Fe^{3+} increases the inhibition rate to 36%, while 90 mmol L^{-1} Cu^{2+} raises it to 32.4%. Surfactants contribute by forming micelles and interacting with the organic moieties of the functionalized graphene oxide, enabling 0.5 g L^{-1} SDBS to enhance the inhibition efficiency to 35.1%. This formulated decontaminant effectively addresses the limitations of conventional water spray methods—such as high water consumption and incomplete capture—in emergency responses to UDMH leakage, reducing the risk of secondary hazards and offering a practical and effective strategy for managing incidents involving hazardous energetic materials. However, the current investigation primarily focuses on aqueous UDMH systems. The efficacy and safety of this decontaminant in scenarios involving pure UDMH fuel leakage or complex contamination environments—such as those arising from co-exposure with other propellants (*e.g.*, hydrazine mixtures, nitrogen tetroxide)—require further systematic evaluation.

Author contributions

Ying Jia and Zuozhou Hou jointly designed the experiment. Zuozhou Hou and Yuanzheng Huang synthesized the decontaminant and carried out the experimental work. All authors collaboratively analyzed and interpreted the experimental data and characterization results, leading to the formulation of the study's conclusions. Zuozhou Hou drafted the manuscript, which was subsequently revised by Yuanzheng Huang.

Conflicts of interest

There are no conflicts to declare.

Data availability

Data will be available upon request.

Acknowledgements

The authors gratefully acknowledge the financial support from the National Natural Science Foundation of China (No. 52370186).

References

1 I. Radelyuk, A. Zhakupbekova, A. Zhumadildinova, A. Kashtanov and N. Baimatova, *Toxics*, 2025, **13**, 963.
2 X. Bai, X. Ren, R. He, F. N. O. Bruce, Y. Tong, W. Lin, J. Wu, Z. Du, Y. Hu and Y. Li, *J. Phys. Chem. A*, 2025, **129**, 8509–8518.
3 C. Hu, Y. Zhang, Y. Zhou, Z. F. Liu and X. S. Feng, *J. Hazard. Mater.*, 2022, **432**, 128708.
4 N. V. Ul'Yanovskii, D. E. Lakhmanov, I. I. Pikovskoi, D. I. Falev, M. S. Popov, A. Y. Kozhevnikov and D. S. Kosyakov, *Sci. Total Environ.*, 2020, **726**, 138483.
5 J. Li, Y. Zhang, D. Xie, P. Guo, Y. Zhu, X. Wang, S. Zhao, T. Zhang and S. Li, *Sep. Purif. Technol.*, 2026, **392**, 137081.
6 J. Su, Y. Huang, H. Wang, M. Shi, K. Shen and Y. Jia, *Sep. Purif. Technol.*, 2024, **331**, 125588.
7 Y. Zeng and X. Ren, *J. Photochem. Photobiol., A*, 2026, **472**, 116818.
8 H. Y. Wang, Y. Jia, X. M. Lv and K. K. Shen, *J. Mol. Liq.*, 2022, **359**, 119197.
9 Y. Huang, Z. Huang, G. Jin and Y. Guo, *IOP Conf. Ser.:Mater. Sci. Eng.*, 2018, **452**, 22119.
10 W. Wang, T. Guo, M. Chen, Y. Liu, M. Lv, T. Hao, Z. Qu, J. Liu and R. Xu, *Powder Technol.*, 2025, 121717.
11 H. Ruomeng, J. Ying, L. Xiaomeng and H. Y. A. S. Keke, *RSC Adv.*, 2021, **11**, 12583–12594.
12 H. Y. Wang and Y. Jia, *Diamond Relat. Mater.*, 2021, **117**, 108457.
13 Y. S. Kwon, Y. Li and B. Huang, *ES Mater. Manuf.*, 2023, **20**, 812.
14 H. Liu, X. Jing, B. Zhang, W. Wang and L. Wang, *Xiyou Jinshu/Chin. J. Rare Met.*, 2019, **43**, 312–318.
15 Q. Li, L. Lv, W. Song and Z. Chen, Numerical simulation of liquid chlorine tank leak based on FLUENT, *2013 IEEE*

Third International Conference on Information Science and Technology (ICIST), IEEE, 2013, pp. 698–701.
16 A. Sandhu, *Nat. Nanotechnol.*, 2008, DOI: 10.1038/nnano.2008.236.
17 N. Withers, *Nat. Chem.*, 2025, **2**, 605.
18 T. Sakuma, R. Sato, A. Yamaguchi, H. Imai, N. Arai and Y. Oaki, *J. Am. Chem. Soc.*, 2025, **147**, 11564–11573.
19 M. Z. Chai, M. W. An, X. Y. Zhang and P. K. Chu, *Rare Met.*, 2022, **41**, 540–545.
20 H. Y. Wang, Y. Jia, X. M. Lv and K. K. Shen, *J. Mol. Liq.*, 2022, **359**, 119197.
21 T. R. Motlokoa, W. K. Maboya, C. Mbileni-Morema, S. J. Modise and B. J. Okoli, *Desalin. Water Treat.*, 2025, **323**, 101341.
22 P. Mahendia, R. Jangra, M. Karokoti, S. Mahendia and O. P. Sinha, *Energy Storage*, 2025, **7**, e70180.
23 L. Niemann, M. Gruschwitz, A. Cordier, M. Köhne and C. Tegenkamp, *Mater. Res. Express*, 2025, **12**, 45603.
24 F. M. O. Medina, M. J. Avena and M. E. Parolo, *Adsorption*, 2024, **30**, 1–11.
25 J. Batta-Mpouma, G. Kandhola and J.-W. Kim, *Sci. Rep.*, 2023, **13**, 21630.
26 K. Karatasos, G. S. Fanourgakis, I. Zuburtikudis and H. A. Khalifeh, *J. Membr. Sci.*, 2025, **713**, 123361.
27 O. Bagheri, M. Esmkhani, S. Javanshir and B. Aghabarari, *Int. J. Biol. Macromol.*, 2023, **253**, 127432.
28 Y. Choi, B. Pandey, X. X. Li, Y. M. Lee, K. B. Cho and W. Nam, *Bull. Korean Chem. Soc.*, 2021, **57**(40), 18906–18914.
29 S. Nechipurenko, S. Efremov, D. Tokmurzin, M. W. Seo, A. Kaiaidarova, N. Zabara and B. D. Burkitbayeva, *Energy Environ.*, 2025, DOI: 10.1177/0958305X251322898.
30 A. R. Zarei, A. Pedram and H. Rezaeivahidian, *Desalin. Water Treat.*, 2016, **57**, 18906–18914.
31 C. Wang, J. Zhu, G. Xiao, X. Zhou, H. Wang, Q. Zhu, Z. Gao and Y. Cao, *Chem. Eng. J.*, 2024, **496**, 154231.
32 Y. Liu and J. Wang, *Chem. Eng. J.*, 2023, **466**, 143147.
33 J. Z. Kuang, Y. Yang, Z. Zou, W. Yuan, Z. Huang and H. Cheng, *Colloids Surf., A*, 2022, **643**, 128747.
34 L. Sun, K. Zhang, Q. Zhao, Y. Gu, C. Zhou, W. Wang and D. Jing, *Transp. Porous Media*, 2021, **140**, 629–642.
35 D. Zhu, Y. Huang, R. Li, S. Peng, P. Wang and J.-J. Cao, *Environ. Sci. Technol.*, 2023, **57**, 17598–17609.
36 Z. Sun, Y. Liang, Y. Xu and K. Zhang, *Dyes Pigm.*, 2025, **239**, 112764.
37 E. Kirtil and M. H. Oztop, *Chem. Pap.*, 2023, **77**, 2343–2361.
38 R. K. Thomas and J. Penfold, *Soft Matter*, 2025, **21**, 3534–3546.
39 Y. Bai, T. Zhang, H. Lin, X. Liu, D. Guo, S. Li and D. Yan, *Energy*, 2024, **295**, 131018.
40 D. M. Yan, S. Q. Ruan, S. K. Chen, Y. Liu, Y. Tian, H. L. Wang and T. N. YE, *J. Zhejiang Univ., Sci., A*, 2021, **22**, 130–146.
41 S. Wang, L. Wu, L. Hong, X. Li, Y. Wu, Y. Ding and T. Li, *Surf. Technol.*, 2025, **54**, 256–265.